Modeling time-dependent current through electronic open channels using a mixed time-frequency solution to the electronic equations of motion

Alexander Prociuk and Barry D. Dunietz
The University of Michigan, Ann Arbor, Michigan 48109, USA
(Received 23 February 2008; revised manuscript received 20 July 2008; published 14 October 2008)

A nonequilibrium Green's function model based on time-dependent perturbation theory is developed to propagate electronic structure and molecular conductance of extended electrode-molecule-electrode nanostructures. In this model, we use the two-time variable nature of the Kadanoff-Baym equations of motion to formulate a mixed time-frequency representation for the electronic density expressed by the appropriate Green's function ($G^<$). This allows for the dynamical treatment of open systems. Furthermore, highly informative time-dependent Wigner distributions are used to shed light on the features of dynamical observables, such as electron current. Calculations, performed on model systems, resolve the dynamic current into direct and alternating components. The direct current is due to electronic open channels near the Fermi level and the alternating response is due to interference fringes from a superposition of extended states. We analyze the transient conductance with respect to the fundamental system's parameters, the effect of bound states, and the conductance driven by laser-induced coherence affected by detuning due to an applied dc bias. The amplitude of the alternating transient current can be adjusted by reshaping the bias pulse or by controlling the electronic coupling terms. Bound states may yield a persisting oscillating response depending on their relative electronic densities. In the analysis we utilize the calculated highly informative time-dependent current distributions.

DOI: 10.1103/PhysRevB.78.165112 PACS number(s): 73.23.−b, 73.40.−c, 73.63.−b, 85.35.Ds

I. INTRODUCTION

The essence of nanoscience research is the further miniaturization of devices. Molecular electronics serves as a natural continuation of this research, where the aim is to design electronic devices and applications based on structure-function relations defined at the molecular level. The increasing interest in molecular and nanoscale electronics is marked by remarkable strides in the ability to fabricate molecular junctions and to measure their conductance properties.[1–17] These advances are accompanied by the development of computational tools to model conductance at the fundamental level. Computational tools are a key ingredient for generating device scale insight on the processes that affect the electronic transmission.

Most current advanced computational treatments are based on implementing the nonequilibrium Green function (NEGF) formalism, where density-functional theory is used to evaluate the electronic integrals.[18–26] Here, we emphasize that, however, most NEGF implementations describe the conductance at steady state where transient effects are disregarded. A related problem of high interest is the study of conductance under the influence of a time-dependent (TD) perturbation such as an alternating-current (ac) field or a laser field. A large body of research has revealed a host of fascinating quantum effects associated with photoassisted conductance in mesoscopic systems such as absolute negative conductance, Coulomb blockade, and Kondo effects driven by ac fields.[27–33] Even more fundamental is the inability of most treatments to describe deviation from direct current (dc) conductance under steady conditions of molecular or nanoscale electronic channels.[34–36] More recently, ac response to a potential pulse ("ringing" mode) has been associated with the presence of bound states.[37,38] These states are localized to the device. Consequently they do not facilitate resonant tunneling through broadening in contrast to conducting molecular states entangled with the electrodes.

This underlies most of the motivation for implementing TD treatments as an alternative to the widely used NEGF scheme for describing electron transport. Some of these treatments use TD density-functional theory (DFT) formalism.[36,39–48] These TD treatments have the potential to describe time-dependent effects related to the applied potential bias and the transient conductance evolving toward a steady state. However, the coupling of the propagated electronic density to electron baths results with difficulties for achieving reliable modeling. The time propagation of open systems as referred to above is especially challenging due to the need to properly treat dissipation effects. These effects mainly originate from the nonequilibrium nature of the extended systems. The Kadanoff-Baym (K-B) equations of motion (e.o.ms) as defined by the Keldysh contour[49–53] inherently account for all quantum-mechanical states of an *open* system including all ionization states. Namely, all possible occupation numbers are used in averaging through the use of the grand-canonical probability expression. The particle exchange with the baths leads to system equilibration that broadens the device region-based energy states.

A formal expression describing TD conductance based on Keldysh NEGF formalism was developed over a decade ago.[34] In Keldysh formalism, the complexity of the full TD description requires using temporally nonlocal electron-electron interaction self-energy[52,53] (SE) terms. For steady-state descriptions, on the other hand, more tractable one-variable expressions can be used. A full Keldysh NEGF-based approach employing a mixed time-frequency representation by integrating a TD Dyson equation was reported.[54] Treatments that use DFT to describe the electron-electron SEs through a high level mean-field expression in Keldysh formalism were also achieved.[41,45,55] These treat-

ments provide useful insight to the time dependence of the modeled conducting channel responding to different forms of a TD bias pulse.

Most descriptions of dynamic transport, which are based on many-body GF-based formalisms, follow the seminal work of Jauho *et al.*,[34] where a partitioning scheme was utilized for describing the unperturbed system. In this picture the coupling of the two bulks through the device region is turned on only as part of the perturbation to which the dynamical response is studied. In this case, the unperturbed system's components are kept each in thermal isolation. A more meaningful description includes equilibration of the device-based conducting channels with the electron baths infinitely prior to switching on the perturbation. This physically more appropriate nonpartitioned approach was suggested first by Cini[56] for a simple model system and was recently used in several real-time-based propagations.[41,45,57] The equilibration in the initial electronic density accounts for dipoles induced across the different regions. These initial-state effects might be dissipated in the steady-state description (if convergence is achieved). They are, however, crucial for addressing transient effects upon the application of the potential bias perturbation.

The propagated electronic device states undergo broadening to form energy bands due to their coupling to an extended system. Our approach is based on solving the K-B electronic e.o.ms as defined by the Keldysh contour (KC) with SEs defined in the frequency domain. This was performed within the nonpartitioned scheme, where we time propagate an open system with bulk-induced broaden electronic states. In this scheme, the response of the device discrete states to the band structure is directly accounted for by the propagated electronic density.

It is important to emphasize several key ingredients and features of our approach. Our frequency space-based scheme provides a desirable and efficient alternative to procedures which are based on real-time propagation schemes[41,45,57] as difficulties in defining efficient time propagation or stepping techniques are avoided. These difficulties are especially important when dealing with dissipation effects due to open systems. This is achieved here by using SE expressions in the frequency domain and utilizing highly efficient perturbation approaches. In general, the SE models defined in the frequency domain (FD) are also more compact in representing energy-coherence driving time-dependent perturbations, whereas the real-time representations of the SEs result with more complex expressions. Pure real-TD expansions require using (sufficiently) larger models of the bulk for reliably describing electron flow.

We derive a master equation projecting the full system to the device region in the mixed time-frequency representation. An analytical expression is subsequently implemented and used to study TD aspects of the electron transport, where a wide-band type of an approximation is used for describing the bulk. In our approach, we directly calculate the time dependence of frequency resolved current, namely, the Wigner form of the current distribution. This provides the most fundamental physical insight of the device response to the applied potential. We use this formalism to study the TD conductance through model electronic channels. We explicitly show the origin of an ac component due to the temporal effects of the applied dc pulse. Namely, its relation to a ringing response of the current upon an abrupt change of the potential bias was studied. The ac response to a variety of dc bias-switching (turn-on/off) rates is shown to be related to interferences due to superpositions of device-based electronic states. This ac response dissipates with different rates due to bulk-induced quantum dephasing effects.

II. METHODS: TIME-DEPENDENT ELECTRONIC CONDUCTANCE

Quantum many-body theory, as described by the Keldysh formalism,[58] can study the dynamics of systems with varying numbers of particles at the *ab initio* level. This amounts to calculating expectation values of dynamical variables in the grand-canonical picture. This formulation can describe well a quantum-mechanical system coupled to a bath represented by statistical formulation. We begin our derivation by introducing the Keldysh formalism and the related nonequilibrium GFs,[49,50,58] which are then used to express the electronic equations of motion in the following subsection. These two introductory subsections are used in the later parts as the starting point for implementing a time-dependent formalism for describing conductance through electronic bulk-coupled channels. In the third to sixth subsections, we derive the propagation equation for the electronic density, bulk representation aspects, current evaluation, and details of the models implemented. This section is then followed by applying the TD approach to model systems focusing on the conductance through few broadened electronic channels.

A. Introduction to the Keldysh-contour formalism

We begin by considering the Hamiltonian expressed by second quantization field operators, $\hat{\Psi}(\vec{x})$ and $\hat{\Psi}^{\dagger}(\vec{x})$, which destroy or create an electron at $\vec{x}$:

$$\hat{H}(t) = \int d\vec{x}\hat{\Psi}^{\dagger}(\vec{x})h(\vec{x},t)\hat{\Psi}(\vec{x}) + \int d\vec{x}\int d\vec{x}'\hat{\Psi}^{\dagger}(\vec{x})\hat{\Psi}^{\dagger}(\vec{x}')J(\vec{x},\vec{x}')\hat{\Psi}(\vec{x})\hat{\Psi}(\vec{x}'). \quad (1)$$

In this expression J corresponds to two-particle interactions and h is the one-particle Hamiltonian, which includes the kinetic energy and a possible time-dependent applied external perturbation $[v(\vec{x},t)]$. Below we specialize our treatment to the case of electrons, where the anticommutation rules apply to these operators.

We now assume that the finite electronic system is coupled to electron reservoirs (baths). For a grand-canonical ensemble the number of electrons is not conserved. At thermal equilibrium, however, the average number of electrons is constant. The corresponding density and partition function are

$$\hat{\rho}_{\circ} = \exp[-\beta(\hat{H} - \mu\hat{N})]/Z, \quad Z = \mathrm{Tr}\{\hat{\rho}_{\circ}\}. \quad (2)$$

We emphasize that the trace is over all possible particle numbers. At the initial steady state the trace $(\mathrm{Tr}\{\hat{\rho}_{\circ}\hat{O}\})$ describes

FIG. 1. The Keldysh contour.

the expectation value of the operator ($\hat{O}$) for the unperturbed (isolated) system with the density operator $\hat{\rho}_\circ$ defined over a complete set of states in the Hilbert space.

We now consider the TD Schrodinger equation (TDSE) in the Heisenberg picture. Let $H(t)$ be the Hamiltonian of a system, which remains at equilibrium up to $t_\circ$, when it is being perturbed:

$$\hat{H}(t < t_\circ) = \hat{H}_\circ. \tag{3}$$

In the Heisenberg representation the time evolution of the expectation value of $\hat{O}$ (for $t > t_\circ$) is

$$O(t) = \langle \hat{O}_H(t) \rangle \equiv \mathrm{Tr}\{\hat{\rho}_\circ \hat{U}(t_\circ, t)\hat{O}\hat{U}(t, t_\circ)\}, \tag{4}$$

where $\hat{U}(t,t')$ is the time evolution operator which relates the solution of the TDSE at time t to time t':

$$|\Psi(t)\rangle = \hat{U}(t,t')|\Psi(t')\rangle. \tag{5}$$

This can be used now, after assuming that $\hat{H}$ and $\hat{N}$ commute to reexpress $\hat{\rho}_\circ = \hat{U}(t_0 - i\beta, t_0)$. Therefore, the time evolution of a $\hat{O}$ is

$$O(t) = \frac{\mathrm{Tr}\{\hat{U}(t_0 - i\beta, t_0)\hat{U}(t_0, t)\hat{O}\hat{U}(t, t_0)\}}{\mathrm{Tr}\{\hat{U}(t_0 - i\beta, t_0)\}}. \tag{6}$$

Thus, the time variable can be analytically continued to the complex plane (Fig. 1) provided that the Hamiltonian is shifted by the chemical potential μ: $\hat{H} \to \hat{H}_G \equiv \hat{H} - \mu\hat{N}$, where $\hat{N}$ is the particle-number operator. The resulting complex time contour (Fig. 1) is referred to as the KC.[58] The KC relates a dynamic electronic system experiencing a time-dependent perturbation to its thermally equilibrated initial state. Several operators which properly propagate the system can be defined by choosing branches on the contour. This results with the formulation of the electronic equations of motion, which are often referred to as the K-B equations.[49,51] These are used in the following subsection in developing our implementation for describing electronic current. Further general details of this formalism can be found elsewhere.[59]

B. Electronic equations of motion

The central quantities of Keldysh and NEGF formalisms are the one-body Green's functions (GFs) (Refs. 49, 50, and 60) or propagators, which are functions of two space-spin and time coordinates ($x = \vec{x}, t$), with time variables defined on the Keldysh contour (Fig. 1). The need for the two variables is a direct consequence of the nature of the electronic structure, which involves two-body electrostatic Coulomb interactions. These two-time variables are ordered on the contour, where their relative positions determine the type of GF. The propagators are defined by the pair of field operators [$\hat{\Psi}(\vec{x})$ and $\hat{\Psi}^\dagger(\vec{x}')$] at times t and t', respectively:

$$G(x,x') \equiv -i\frac{\mathrm{Tr}[\hat{U}(t_0 - i\beta, t_0)\hat{\mathcal{T}}_C[\hat{\Psi}_H(x)\hat{\Psi}_H^\dagger(x')]]}{\mathrm{Tr}[\hat{U}(t_0 - i\beta, t_0)]}. \tag{7}$$

In the Heisenberg picture, these operators take the form

$$\hat{\Psi}_H(x) = \hat{U}(t_\circ, t)\hat{\Psi}(\vec{x})\hat{U}(t, t_\circ). \tag{8}$$

The contour ordering operator, $\hat{\mathcal{T}}_C$, can be expanded, allowing the GF to be expressed as a sum over two types of GFs related to the relative positions of the two-time variables on the contour:

$$G(x,x') = \theta(t,t')G^>(x,x') + \theta(t',t)G^<(x,x'), \tag{9}$$

where the step function, $\theta(t,t')$, is one if t is later than t' on the Keldysh contour. This does not necessarily imply that $t > t'$ on the real-time axis. The contour has on the real axis a forward branch $(t_\circ, t)$, a backward branch $(t, t_\circ)$, and a branch along the imaginary axis at $t_\circ$ $(t_\circ, t_\circ - i\beta)$. This results in seven GFs, depending on the particular order and choice of the branches to which the two-time variables belong.

The different K-B equations are related to each other through analytic continuation as set forth by the KC. Here we focus on the $G^<$, which provides the electronic density through: $\rho(x) = -i \lim_{x' \to x} G^<(x,x')$ (x, x' are space-time variables, as defined above). The one-particle K-B e.o.m of $G^<$ includes explicit two-body interactions (i.e., electron-electron repulsions) through SE (Refs. 49, 50, 52, and 53) functions (Σ), which are, in general, functions of the GF. Here, we are neglecting electron-electron SE interaction terms. The complete one-body Hamiltonian takes the following form:

$$h(x) = h_0(\vec{x}) + v(x), \tag{10}$$

with $v(x)$ being the time-dependent external potential acting on the electrons, and $h_0(\vec{x})$ represents the electron kinetic energy and electron-nuclear attractions. The influence of the coupled extended electronic systems (the electrodes) can be represented through appropriate SE terms as detailed below.

We start with the KB equation and conjugation relation for the lesser GF [Eqs. (11) and (12)]. The time variables in these equations are on the real branches of the Keldysh contour:

$$\left[i\frac{\partial}{\partial t} - h(x)\right]G^<(x,x') = 0, \tag{11}$$

$$[G^<(x,x')]^* = -G^<(x',x). \tag{12}$$

Localized basis functions are used to represent the different operators. These basis functions are used for defining the projection of the influence of the bulk on the device region. The unperturbed equilibrated system is described in this representation as discussed in detail below. Here, we focus on the propagated $G^<$, which is expressed in this linear combination of atomic orbital (LCAO) basis as

$$G^<(x,x') = \sum_{i,j} G^<_{i,j}(t,t')\phi_i(\vec{x})\phi_j(\vec{x}'), \tag{13}$$

and $h_{i,j}(t) = \int d\vec{x}\phi_i(\vec{x})h(x)\phi_j(\vec{x})$. In this representation we also write the overlap of the nonorthogonal basis functions as $S_{i,j} = \int d\vec{x}\phi_i(\vec{x})\phi_j(\vec{x})$. The system is propagated in an orthogonalized basis where $\mathbf{h}$ and $\mathbf{S}$ commute. This transforms Eqs. (11) and (12) to

$$\left[i\mathbf{1}\frac{\partial}{\partial t} - \mathbf{h}(t) \right]\mathbf{G}^<(t,t') = 0, \tag{14}$$

$$[\mathbf{G}^<(t,t')]^\dagger = -\mathbf{G}^<(t',t). \tag{15}$$

Conjugate transposing Eq. (14) and substituting Eq. (15) gives

$$-i\frac{\partial}{\partial t'}\mathbf{G}^<(t,t') - \mathbf{G}^<(t,t')\mathbf{h}(t') = 0. \tag{16}$$

Next, we combine Eqs. (14) and (16) by rewriting in terms of the time variables: $\bar{t} \equiv \frac{t_1+t_2}{2}$ and $\Delta t \equiv t_1 - t_2$, and noting that $\partial/\partial\bar{t} = \partial/\partial t_1 + \partial/\partial t_2$:

$$\frac{\partial}{\partial \bar{t}}\mathbf{G}^<(\bar{t},\Delta t) = i\left[\mathbf{G}^<(\bar{t},\Delta t)\mathbf{h}\left(\bar{t} - \frac{\Delta t}{2}\right) - \mathbf{h}\left(\bar{t} + \frac{\Delta t}{2}\right)\mathbf{G}^<(\bar{t},\Delta t) \right]. \tag{17}$$

C. Propagation in a mixed time-frequency representation

The brute force solution of an expansion involving two-time-domain variables is computationally intensive [Eqs. (14), (16), and (17)]. Most steady-state descriptions, on the other hand, utilize the ability to simplify the expression by collapsing the two-time variables to a single time difference variable. Pure time-domain representations require using sufficiently large clusters to reliably treat conductance through a device region. In the frequency domain, on the other hand, self-energy expressions can use a cluster model to effectively represent any open system. Here we note that the convergence of bulk-coupling self-energy models with their size has been analyzed by us.[61] Frequency domain bulk-SE models are employed in our TD approach.

We now consider introducing a frequency-domain variable by Fourier transforming the above time-domain expression. The combination of the two adjoined K-B equations [Eq. (17)] facilitates the use of time-dependent perturbation theory (PT) as the propagation method. A generalized Fourier transform operator ($\mathcal{F}$):

$$\begin{aligned}\mathcal{F}[f(\Delta t)] &\equiv \int_{-\infty}^{\infty} d(\Delta t)[e^{i(\bar{\omega}+i\eta)\Delta t}\Theta(\Delta t) \\ &\quad + e^{i(\bar{\omega}-i\eta)\Delta t}\Theta(-\Delta t)]f(\Delta t) \\ &\equiv f_1(\bar{\omega}) + f_2(\bar{\omega}) \equiv f(\bar{\omega}),\end{aligned} \tag{18}$$

where $\eta \to 0^+$, leads when applied on $G^<(\bar{t},\Delta t)$ to

$$\mathbf{G}^<(\bar{t},\bar{\omega}) = \mathbf{G}^<_1(\bar{t},\bar{\omega}) + \mathbf{G}^<_2(\bar{t},\bar{\omega}), \tag{19}$$

where

$$\mathbf{G}^<_1(\bar{t},\bar{\omega}) = \int_{-\infty}^{\infty} d(\Delta t)e^{i(\bar{\omega}+i\eta)\Delta t}\Theta(\Delta t)\mathbf{G}^<(\bar{t},\Delta t),$$

$$\mathbf{G}^<_2(\bar{t},\bar{\omega}) = -\mathbf{G}^{\dagger<}_1(\bar{t},\bar{\omega}). \tag{20}$$

The use of the two branches, where Θ is the step function, ensures that the transformed function approaches zero as Δt approaches $\pm\infty$.

We now focus on the e.o.m. for the transformed GF: $\mathbf{G}^<(\bar{t},\bar{\omega})$. This mixed time-frequency representation, as used below, provides substantial physical insight into the electronic response aspects of the propagated model system. The generalized FT [Eq. (18)] is applied to the reexpressed time-domain K-B equation [Eq. (17)]. Here, the actual transformed quantities take the following form: $\mathcal{F}[\mathbf{v}(\bar{t}+\Delta t/2)\mathbf{G}^<(\bar{t},\Delta t)]$ and $\mathcal{F}[\mathbf{G}^<(\bar{t},\Delta t)\mathbf{v}(\bar{t}-\Delta t/2)]$. There are four such terms to be transformed where, for example, by using standard FT relations:

$$\begin{aligned}&\int_{-\infty}^{\infty} d(\Delta t)e^{i(\omega+i\eta)\Delta t}\mathbf{v}\left(\bar{t}+\frac{\Delta t}{2}\right)\mathbf{G}^<(\bar{t},\Delta t)\Theta(\Delta t) \\ &\quad = \int_{-\infty}^{\infty} d\omega'\mathbf{v}(\bar{t},\omega')\mathbf{G}^<_1(\bar{t},\bar{\omega}-\omega'),\end{aligned} \tag{21}$$

and

$$\mathbf{v}(\bar{t},\bar{\omega}) = \frac{1}{\pi}e^{-i2\bar{\omega}\bar{t}}\int_{-\infty}^{\infty} dt e^{i(2\bar{\omega})t}\mathbf{v}(t) = \frac{1}{\pi}e^{-i2\bar{\omega}\bar{t}}\tilde{\mathbf{v}}(2\bar{\omega}). \tag{22}$$

This is performed on all terms expressed by $\mathbf{G}_1$ and $\mathbf{G}_2$, where by symmetry the resulting e.o.m. becomes

$$\begin{aligned}\frac{\partial}{\partial \bar{t}}\mathbf{G}^<(\bar{t},\bar{\omega}) &= i[\mathbf{G}^<(\bar{t},\bar{\omega}),\mathbf{h}_0] + i\int d\omega'[\mathbf{G}^<(\bar{t},\bar{\omega}+\omega')\mathbf{v}(\bar{t},\omega') \\ &\quad - \mathbf{v}(\bar{t},\omega')\mathbf{G}^<(\bar{t},\bar{\omega}-\omega')].\end{aligned} \tag{23}$$

This relation is accurate also for nonvanishing η values. Here, both the perturbation $\mathbf{v}(t)$ and $\mathbf{h}_0$ are Hermitian as they still represent the full (nontruncated) system. Furthermore, we rewrite $\mathbf{G}^<(\bar{t},\bar{\omega})$ as the sum of a contribution in the absence of a perturbation $\mathbf{G}^{0,<}(\bar{\omega})$ and the remainder $\Delta\mathbf{G}^<(\bar{t},\bar{\omega}) \equiv \mathbf{G}^<(\bar{t},\bar{\omega}) - \mathbf{G}^{0,<}(\bar{\omega})$. The $\mathbf{G}^{0,<}(\bar{\omega})$ is $\bar{t}$ independent by definition of the GF [Eq. (7)]. This allows us to rewrite Eq. (23) in a form suitable for TD PT where the zeroth order term is the lesser GF in the absence of a perturbation (see Appendix for further discussion):

$$\frac{\partial}{\partial \bar{t}}\Delta\mathbf{G}^{<}(\bar{t},\bar{\omega}) = i[\Delta\mathbf{G}^{<}(\bar{t},\bar{\omega}),\mathbf{h}_0] + i\int d\omega'[\mathbf{G}^{<}(\bar{t},\bar{\omega}+\omega')\mathbf{v}(\bar{t},\omega') - \mathbf{v}(\bar{t},\omega')\mathbf{G}^{<}(\bar{t},\bar{\omega}-\omega')]. \quad (24)$$

We recast Eq. (23) into an iterative equation by writing $\mathbf{G}^{<}(\bar{t},\bar{\omega})$ as a dressed form,

$$\Delta\mathbf{G}^{<}(\bar{t},\bar{\omega}) = \mathbf{e}^{-i\mathbf{h}_0(\bar{t}-t_0)}\Delta\mathcal{G}^{<}(\bar{t},\bar{\omega})\mathbf{e}^{i\mathbf{h}_0(\bar{t}-t_0)}, \quad (25)$$

thus eliminating the terms with $\mathbf{h}_0$ in Eq. (23) and leaving only the perturbing terms with $\mathbf{v}(\bar{t},\bar{\omega})$. The resulting time-differential equation is expressed as

$$\frac{\partial}{\partial \bar{t}}\mathcal{G}^{<}(\bar{t},\bar{\omega}) = i\int_{-\infty}^{\infty} d\omega' \mathbf{e}^{i\mathbf{h}_0(\bar{t}-t_0)}[\mathbf{G}^{<}(\bar{t},\bar{\omega}+\omega')\mathbf{v}(\bar{t},\omega') - \mathbf{v}(\bar{t},\omega')\mathbf{G}^{<}(\bar{t},\bar{\omega}-\omega')]\mathbf{e}^{-i\mathbf{h}_0(\bar{t}-t_0)}. \quad (26)$$

Integrating provides

$$\mathcal{G}^{<}(\bar{t},\bar{\omega}) = \mathcal{G}^{<}(t_\circ,\bar{\omega}) - i\int_{-\infty}^{\bar{t}} d\bar{t}' \int d\omega' \times\{\mathbf{e}^{i\mathbf{h}_0(\bar{t}'-t_0)}[\mathbf{G}^{<}(\bar{t}',\bar{\omega}+\omega')\mathbf{v}(\bar{t}',\omega') - \mathbf{v}(\bar{t}',\omega')\mathbf{G}^{<}(\bar{t}',\bar{\omega}-\omega')]\mathbf{e}^{-i\mathbf{h}_0(\bar{t}'-t_0)}\}. \quad (27)$$

Hence, the solution for this e.o.m. by time-dependent perturbation expansion is provided by

$$\mathbf{G}^{<}(\bar{t},\bar{\omega}) = \mathbf{G}^{0,<}(\bar{\omega}) + i\int_{t_0}^{\bar{t}} d\bar{t}' \times e^{-i\mathbf{h}_0(\bar{t}-\bar{t}')}\int d\omega'[\mathbf{G}^{<}(\bar{t}',\bar{\omega}+\omega')\mathbf{v}(\bar{t}',\omega') - \mathbf{v}(\bar{t}',\omega')\mathbf{G}^{<}(\bar{t}',\bar{\omega}-\omega')]\mathbf{e}^{i\mathbf{h}_0(\bar{t}-\bar{t}')}. \quad (28)$$

We note through an appropriate choice of $\mathbf{h}_0$ as discussed above, $\mathbf{G}^{<}(\bar{t},\bar{\omega})=\mathbf{G}^{0,<}(\bar{\omega})$ in the absence of a perturbation. Thus, $\bar{t}$ independence of the initial GF is satisfied and no TD artifacts are introduced at the unperturbed conditions.

Here we also note that h_0 represents the full system and is still assumed to be Hermitian. However, upon defining a finite space for propagation and due to coupling to the bulks, non-Hermitian terms have to be added to the propagation Hamiltonian. In the next subsection we implement a master equation, which properly represents the bulk effects within a finite (device) region. In treating molecular or nanoscale electron transport, one naturally refers to the device region as the propagated space under the effect of coupling to the two electrodes.

D. Simulating semi-infinite electrodes

For description of TD conductance the electronic density at the unperturbed state has to be properly evaluated for defining the initial conditions of the propagation. The initial $\mathbf{G}_0^{<}$ (i.e., the unperturbed equilibrated system) must describe well the steady state, which is thermally equilibrated with the electron baths. We remind that, in this physically proper non-partitioned view,[56] the different subsystems are allowed to reach thermal equilibration as one system. Namely, their coupling is not part of the turned on perturbation. This has been highlighted by several recent studies.[41,45,57]

The Keldysh formalism is used to properly account for the thermal equilibration of the device with the electrodes. This is achieved by a Matsubara GF (G^M), which corresponds entirely to the imaginary part of the Keldysh contour. Through KC continuation

$$G^M \rightarrow G^{<}(t_0,t_0) \equiv G_0^{<}, \quad (29)$$

an expression for the $G^{<}$ at steady state is obtained from the G^M. A proper treatment of the steady state including a solution of the G^M is required to allow any dc response. This is essentially equivalent to imposing the grand-canonical picture to allow for particle exchange between the coupled system and bath. In the absence of a perturbation, $\mathbf{G}^{<}(\bar{t},\bar{\omega}) = \mathbf{G}^{\mathbf{0},<}(\bar{\omega}) = \mathbf{G}_{\mathbf{1}}^{\mathbf{0},<}(\bar{\omega}) - \mathbf{G}_{\mathbf{1}}^{\mathbf{0},<\dagger}(\bar{\omega})$, where

$$\mathbf{G}_{\mathbf{1}}^{\mathbf{0},<}(\bar{\omega}) = i\mathbf{G}^{\mathbf{R}}(\bar{\omega})\mathbf{G}_{\mathbf{0}}^{<} = -\mathbf{G}^{\mathbf{R}}(\bar{\omega})\mathbf{f}(\mathbf{h}_0-\mu I). \quad (30)$$

Here, the Fermi matrix $\mathbf{f}(\mathbf{A})$ is a function of a matrix and in the limit of noninteracting electrons is given by $\mathbf{f}(\mathbf{A}) = e^{-\beta\mathbf{A}}[\mathbf{I}+e^{-\beta\mathbf{A}}]^{-1}$, assuming $\mathbf{A}$ is Hermitian. This condition is satisfied for the orthogonalized basis set, where $\mathbf{h}_0 = \mathbf{S}^{-1/2}\bar{\mathbf{h}}\mathbf{S}^{-1/2}$. The Fermi matrix above provides an analytical solution for the G^M in the case of noninteracting electrons. Here, for clarity, we distinguish between the Hamiltonian in the orthogonal basis, h, from the Hamiltonian expressed in the localized atomic orbital (AO) basis $\bar{h}$. We will use, in the following sections, the localized basis for defining a device region and to describe its coupling to extended bulk regions. More specifically, we evaluate the unperturbed system in the localized basis, whereas the propagation relations are all implemented in the orthogonalized representation. These are also the bases by which the related equations are expressed in.

For a Hamiltonian of a closed system represented in a finite basis, $\mathbf{G}^{0,<}(\bar{\omega})$ is diagonal in the basis that diagonalizes $\bar{\mathbf{h}}$. This implies that $\mathbf{G}^{0,<}(\bar{\omega})$ does not introduce any off-diagonal coherences and represents a purely equilibrated system. On the other hand, an open system introduces a nontrivial $\bar{\omega}$ dependence to the Hamiltonian (in the form of bulk SEs). In this case, $\mathbf{G}^{0,<}(\bar{\omega})$ can still be diagonalized by a different unitary operator at each $\bar{\omega}$ provided that $\mathbf{G}^{R}(t_0,\bar{\omega})$ and $\mathbf{f}$ depend on $\mathbf{h_0}(\bar{\omega})$. This amounts to propagating an initially decoherent statistical ensemble at each $\bar{\omega}$. If, on the other hand, the initial-state description involves a $\mathbf{G}^{R}(\bar{\omega})$ that depends on $\mathbf{h_0}(\bar{\omega})$ and the Fermi matrix ($\mathbf{f}$) that depends on the cluster $\mathbf{h_0}$, this initial-state description is not guaranteed to be diagonalizable at each $\bar{\omega}$. This introduces additional coherence effects at perturbation turn on. We emphasize that this still will not introduce $\bar{t}$-dependent artifacts in the absence of a perturbation by construction. Furthermore, the initial guess is guaranteed not to correspond to arbitrarily turning on the electron density of the leads at $\bar{t}=t_0$ since $\bar{\omega}$ depends on all Δt.

We focus, now, specifically on transport-related dissipation effects. There are several mechanisms which contribute to dissipation of the current flow. These include optical lifetimes, thermal decay due to interelectron interactions, and quantum dephasing from the coupling to semi-infinite electrodes. Optical lifetimes in most systems are usually long compared to thermal and electrode bath lifetimes, and can often be neglected. Thermal decay is, in fact, treated within the Keldysh formalism by a second-order expansion of the electron correlation self-energy (which we neglect in this report). To accurately include the remaining dissipation effect due to quantum dephasing emerging from the coupled electron baths is still a challenging task. Our approach is based on purely quantum propagation of an *initially* grand-canonical ensemble [see Eq. (4) and related derivation]. This is achieved by deriving a quantum master equation (rate equation).

For deriving the projected master equation we represent the effects of the bulks by SE expressions. Electrode SE expressions are widely used in formalisms implementing the Landauer approach and its more sophisticated NEGF extension. In these schemes, which are formulated in the frequency domain, the Hamiltonian of a cluster model is subdivided into three regions. The subspaces within the cluster model include two surface regions connected by the device region. The bulk electrodes are represented explicitly by SE terms, where, for example, the left electrode is described by

$$\bar{\boldsymbol{\Sigma}}_l = (E\mathbf{S_{cl}} - \bar{\mathbf{h}}_{\mathbf{cl}})\bar{\mathbf{g}}^r_{\mathbf{ll}}(\bar{\omega})(E\mathbf{S_{lc}} - \bar{\mathbf{h}}_{\mathbf{lc}}). \tag{31}$$

The evaluation of the initial state also requires evaluating the electrode's surface GFs, $\bar{\mathbf{g}}^{\mathbf{R}}_{\{\mathbf{ll},\mathbf{rr}\}}(\bar{\omega})$. This is described in the next subsection.

To complete the description of the unperturbed (equilibrated) system, the G^R_{cc} is evaluated as usual by inversion of the Hamiltonian with the SE added to represent the bulk-induced broadening effects:

$$\bar{\mathbf{G}}^{\mathbf{R}}_{\mathbf{cc}}(\omega) = [(\omega + i\eta_d)\mathbf{S_{cc}} - \bar{\mathbf{h}}_{\mathbf{cc}} - \bar{\boldsymbol{\Sigma}}_{\mathbf{l}}(\omega) - \bar{\boldsymbol{\Sigma}}_{\mathbf{r}}(\omega)]^{-1}, \tag{32}$$

where the infinite nature of the system is represented by adding the bulk SEs to the Hamiltonian defined within a finite region. This amounts to

$$\mathbf{h}_0 \to \mathbf{h_{cc}} + \boldsymbol{\Sigma} = \mathbf{h_{cc}} + \mathbf{1/2}(\boldsymbol{\Sigma} + \boldsymbol{\Sigma}^\dagger) + \mathbf{1/2}(\boldsymbol{\Sigma} - \boldsymbol{\Sigma}^\dagger), \tag{33}$$

where a non-Hermitian component for the Hamiltonian is now included. This associates finite lifetimes to the scattering states within the device region. A general master equation to project onto the device region is derived by rewriting Eq. (23):

$$\begin{aligned} i\frac{\partial}{\partial \bar{t}}\Delta\mathbf{G}^<_{cc}(\bar{t},\bar{\omega}) &= [\mathbf{h}_{cc}, \Delta\mathbf{G}^<_{cc}(\bar{t},\bar{\omega})] \\ &+ \int d\omega' [\mathbf{v_{cc}}(\bar{t},\omega')\mathbf{G}^<_{cc}(\bar{t},\bar{\omega}-\omega') \\ &- \mathbf{G}^<_{cc}(\bar{t},\bar{\omega}+\omega')\mathbf{v_{cc}}(\bar{t},\omega')] \\ &+ \int_{-\infty}^{\infty} dt' [\boldsymbol{\Sigma}^{\mathbf{R}}(\bar{t}-t')\Delta\mathbf{G}^<_{\mathbf{cc}}(t',\bar{\omega})e^{-i\mathbf{h_{cc}}(\bar{t}-t')} \\ &- e^{i\mathbf{h_{cc}}(\bar{t}-t')}\Delta\mathbf{G_{cc}}(t',\bar{\omega})\Sigma^A(t'-\bar{t})]. \end{aligned} \tag{34}$$

The subscript cc refers to the device central subspace and $G^<_{cc}(\bar{t},\bar{\omega}) = G^{0,<}_{cc}(\bar{\omega}) + \Delta G^<_{cc}(\bar{t},\bar{\omega})$. The full derivation of the last equation is provided in the Appendix.

E. Models

The steady state defines the unperturbed system and therefore serves as the initial point of the time propagation treatment. The proper thermalization of the full system has to be treated well in the $\mathbf{G}^{0,<}(\bar{\omega})$ as explained above using the SEs [Eqs. (29) and (30)]. We comment also that the projected Fermi matrix to the device region needs to include correction terms due to the coupling to the bulk:

$$\bar{\mathbf{f}} \to \bar{\mathbf{f}}_{\mathbf{cc}} - (\bar{\omega}\mathbf{S_{cl}} - \bar{\mathbf{h}}_{\mathbf{cl}})\bar{\mathbf{g}}^{\mathbf{R}}_{\mathbf{ll}}\bar{\mathbf{f}}_{\mathbf{lc}} - (\bar{\omega}\mathbf{S_{cr}} - \bar{\mathbf{h}}_{\mathbf{cr}})\bar{\mathbf{g}}^{\mathbf{R}}_{\mathbf{rr}}\bar{\mathbf{f}}_{\mathbf{rc}}. \tag{35}$$

These terms are found to involve a negligible effect with the models used below.

The electronic density propagation is specialized to the mixed representation. In this representation an analytical expression, as derived next, is obtained within a wide-band-limit (WBL) treatment. This WBL is appropriate for analyzing the dependence of the transient transport on the key parameters of the electronic channels.

The Hamiltonian used to generate a wide-band approximation to the bulk density of states (DOS) has (subject to a chemical potential, μ_0) the form $\mathbf{h}_0 \sim (\bar{\omega} - \mu_0)\mathbf{S}$. One can easily show that, for such a Hamiltonian, the retarded GF has a wide-band-limit representation of the form

$$\mathbf{g}^{\mathbf{R}}_{\mathbf{l}} = \frac{1}{\mu_0 + i\eta_b}\mathbf{S}^{-1}_{\mathbf{ll}}, \tag{36}$$

where an equivalent $\mathbf{g}^{\mathbf{R}}_{\mathbf{rr}}$ for the right electrode is also used. For convenience the Fermi energy of the bulk (μ_0) is set to zero. We also represent finite bandwidth aspects by setting the surface GF to zero at energy regions beyond the modeled band structure. This is essential for studying bound states included in the device region (with energies beyond the surface band structure) as analyzed below.

We simplify the SE expressions by assuming

$$\boldsymbol{\Sigma}(\mathbf{t}) = \boldsymbol{\Sigma}_{\mathbf{0}}\delta(\mathbf{t}). \tag{37}$$

The general master equation in the mixed representation [Eq. (34)] takes the following form:

$$\begin{aligned} i\frac{\partial}{\partial \bar{t}}\Delta\mathbf{G}^<_{cc}(\bar{t},\bar{\omega}) &= [(\mathbf{h}_{cc} + \boldsymbol{\Sigma}^{\mathbf{R}}_{\mathbf{0}})\Delta\mathbf{G}^<_{cc}(\bar{t},\bar{\omega}) \\ &- \Delta\mathbf{G}^<_{cc}(\bar{t},\bar{\omega})(\mathbf{h}_{cc} + \boldsymbol{\Sigma}^{\mathbf{A}}_{\mathbf{0}})] \\ &+ i\int_{-\infty}^{\infty} d\omega' [\mathbf{v_{cc}}(\bar{t},\omega')\mathbf{G}^<_{cc}(\bar{t},\bar{\omega}-\omega') \\ &- \mathbf{G}^<_{cc}(\bar{t},\bar{\omega}+\omega')\mathbf{v_{cc}}(\bar{t},\omega')]. \end{aligned} \tag{38}$$

This transforms the imaginary part of the general relation [Eq. (28)] by the appropriate decay factor. This leads to a time propagation equation, which is the WBL form of the general master equation [see Eq. (34)]:

$$\mathbf{G}_{cc}^{<}(\bar{t},\bar{\omega}) = \mathbf{G}_{cc}^{0,<}(\bar{\omega}) + i\int_{t_0}^{\bar{t}} d\bar{t}'\, \mathbf{e}^{-i(\mathbf{h}_{cc}+\boldsymbol{\Sigma}_0^{\mathbf{R}})(\bar{t}-\bar{t}')} \times \int d\omega' [\mathbf{G}_{cc}^{<}(\bar{t}',\bar{\omega}+\omega')\mathbf{v}_{\mathbf{cc}}(\bar{t}',\omega') - \mathbf{v}_{\mathbf{cc}}(\bar{t}',\omega') \times \mathbf{G}_{cc}^{<}(\bar{t}',\bar{\omega}-\omega')]\mathbf{e}^{i(\mathbf{h}_{cc}+\boldsymbol{\Sigma}_0^{\mathbf{A}})(\bar{t}-\bar{t}')}. \quad (39)$$

The complexity in this expression is due to the convolution integral in $\bar{\omega}$ and the infinite nature of the system contributing dissipation effects. We use TD perturbation theory to simplify the full propagation solution for $[\mathbf{G}^{<}(\bar{t},\bar{\omega})]$. The first-order treatment corresponds to single-photon transition dynamics, or alternatively, yields the conductance at zero bias for a simple potential bias perturbation. A second-order expansion is required to treat two photon excitations. The first-order TD expansion of the GF is

$$\mathbf{G}_{cc}^{<}(\bar{t},\bar{\omega}) = \mathbf{G}_{cc}^{0,<}(\bar{\omega}) + i\int_{t_0}^{\bar{t}} d\bar{t}'\, \mathbf{e}^{-i(\mathbf{h}_{cc}+\Sigma_0^{R})(\bar{t}-\bar{t}')} \times \int d\omega' [\mathbf{G}_{cc}^{0,<}(\bar{\omega}+\omega')\mathbf{v}_{cc}(\bar{t}',\omega') - \mathbf{v}_{cc}(\bar{t}',\omega') \times \mathbf{G}_{cc}^{0,<}(\bar{\omega}-\omega')]\mathbf{e}^{i(\mathbf{h}_{cc}+\Sigma_0^{A})(\bar{t}-\bar{t}')}, \quad (40)$$

where $\mathbf{G}_{cc}^{0,<}(\bar{\omega})$ is the propagated (zeroth order) GF. At any given time step, $\bar{t}=t_n$, $\mathbf{G}^{<}(\bar{t},\bar{\omega})$ can be updated from the previous time step, t_{n-1}, with a proper shift by the propagator. We also note that a larger time step in the simulation corresponds to fewer frequency-domain data points in the convolution integral. This leads to an efficient and manageable simulation. Here, this mixed representation is used in evaluating the current on a model system as described next.

We concentrate in this study on the TD conductance effect through a one-dimensional wire composed of hopping sites. We assume a tight-binding scenario where interactions are included only between neighbor sites. The device region is defined after dividing the system to three regions, where the central region is the device bonded to two semi-infinite bulk wires. In the results reported below we include two sites to define the device region. An illustration of this system along with the relevant electronic parameters is provided in Fig. 2. We note that β and s are the electronic and overlap coupling terms. The diagonal terms of the model Hamiltonian are set to the initial Fermi energy of the system. Accordingly, we express the current operator (see Sec. III for further detailed discussion) with the numerical values assigned to the electronic integrals in the Hamiltonian

$$\mathbf{O} = \mathbf{i}\begin{bmatrix} 0 & \beta_d \\ -\beta_d & 0 \end{bmatrix}. \quad (41)$$

In all calculations reported below in Sec. III we set the FE to zero ($\mu_0=0$). This also defines the on site energies as described in the figure. We have also used, for the electronic coupling terms unless differently specified: $\beta_d=0.25$ eV, $\beta_l=\beta_r=0.25$ eV. We use a sufficiently small value ($\eta_d=0.005$ eV) for the fundamental broadening factor added to the imaginary component of the Hamiltonian used to calculate the G_0^R [see Eq. (32)]. This describes the unperturbed equilibrated system. The bulk GF is associated with another fundamental broadening factor (η_b) of effectively 0.025 eV when the mixing parameter is 0.25 eV [see Eq. (36)]. For selectively tuning the broadening of only the open channels and leaving the bound states unaffected, η_b is modified while η_d is kept constant. Finally, we note that in all calculations the target bias potential is set to 0.2 eV.

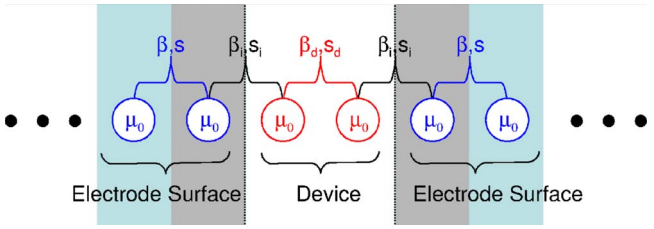

FIG. 2. (Color online) One-dimensional wire composed of an array of hopping sites. The central region corresponds to the device, which can be set to different site to model doping. The coupling terms within the device are denoted as β_d, coupling of the device bulk β_l and β for the bulk region. Corresponding s terms for the overlap are defined as well.

F. Current evaluation

We now describe the evaluation of the current from the time propagated $G^{<}$ function. In the second-quantized representation, most dynamical variables (e.g., dipole, spin, and current operators) can be expressed in terms of one pair of field operators [see also Eq. (4) and (5)]:

$$\hat{O} = \int_{-\infty}^{\infty} d\vec{x}\hat{\psi}^{\dagger}(\vec{x})\mathcal{O}(\vec{x})\hat{\psi}(\vec{x}), \quad (42)$$

where the function $\mathcal{O}(\vec{x})$ is the one-particle case for a many-body operator. For example, given the number density operator for a system of N particles at position $\vec{r}$, where $\Sigma_{n=1}^{N}\delta(\vec{x}_n-\vec{r})$, $\hat{O}$ becomes $\mathcal{O}(\vec{x})=\delta(\vec{x}-\vec{r})$. The grand-canonical expectation value of any dynamical variable [see Eq. (4)] is given by

$$\langle\hat{O}(t_1)\rangle = -i\int_{-\infty}^{\infty} d\vec{x}_1 \lim_{x_2\to x_1}[\mathcal{O}(\vec{x}_1)G^{<}(x_1,x_2)]. \quad (43)$$

Given the basis set representation [Eq. (13)], this expectation value can be expressed as a product of two matrices

$$\langle\mathbf{O}(t_1)\rangle = -i\,\mathrm{Tr}\left\{\lim_{t_2\to t_1}[\mathcal{O}\mathbf{G}^{<}(t_1,t_2)]\right\} = -i\,\mathrm{Tr}\left\{\lim_{\Delta t\to 0,\bar{t}\to t_1}[\mathcal{O}\mathbf{G}^{<}(\bar{t},\Delta t)]\right\} = \mathrm{Tr}\left\{\lim_{\bar{t}\to t_1}\left[\frac{-i}{2\pi}\int_{-\infty}^{\infty} d\bar{\omega}\mathcal{O}\mathbf{G}^{<}(\bar{t},\bar{\omega})\right]\right\}, \quad (44)$$

where $\mathcal{O}_{\mathbf{ij}}=\int_{-\infty}^{\infty}\mathbf{d\tilde{x}}\phi_{\mathbf{i}}(\tilde{\mathbf{x}})\mathcal{O}(\tilde{\mathbf{x}})\phi_{\mathbf{j}}(\tilde{\mathbf{x}})$. Let us now consider the specific case of the current-density operator. One can show that, for this operator,

$$\mathcal{O}(\vec{x}) = -i[\vec{\nabla}_x \delta(\vec{x}-\vec{r}) + \delta(\vec{x}-\vec{r})\vec{\nabla}_x]. \quad (45)$$

The current-density operator is position dependent. It can be expressed in an LCAO basis

$$\mathcal{O}_{ji}(\vec{r}) = i[\phi_i(\vec{r})\vec{\nabla}\phi_j(\vec{r}) - \phi_j(\vec{r})\vec{\nabla}\phi_i(\vec{r})], \quad (46)$$

and, in matrix form, is Hermitian under permutation of the indices i and j. The electron current through a given plane is calculated by tracing $[-i\mathcal{O}\mathbf{G}^<]$. This trace, which is the vector current density defined in an AO basis, is then expressed on a spatial grid. The current is finally obtained by integrating over the plane, which is perpendicular to the flux direction.

III. RESULTS

The conductance due to electronic transmittance through a single-quantum channel is analyzed for transient effects. We use the parameters as listed in Sec. II E, where only η_b is effectively increased by a factor of 3. We start by demonstrating the dramatic effect of the applied time-shaped potential pulse. In Fig. 3, conductance due to four potential pulses is provided. In all cases, for convenience, sufficiently slow turn-on events (elapsing 15 fs) are followed by differing time durations at the target bias and/or differing turn-off rates. (The 15 fs corresponds to about three periods of a system characterized by 1 eV transition energy. We analyze below in detail its relative adiabaticity as determined in reference to other system parameters.) The responding current evolves to steady state upon a long enough constant bias. We study the effect of turning off the pulse adiabatically versus applying an abrupt perturbation on the achieved steady-state current under the target potential bias. All potential switching slopes are defined by one quarter of a sinus function stretched over different time periods and, therefore, are described by continuous and analytical functions. The actual potential ramping profiles are illustrated in the left of the figure. An additional curve which includes also bound states is provided for comparison.

First we draw attention to the current under constant potential bias. All $I(t)$ curves achieve the same steady-state current, as expected, since all ramping potentials are set to the same bias target. The related steady-state currents are evaluated by $I(V)=\frac{V}{2}g_0(\frac{\beta_d\Sigma}{(\beta_d^2+\Sigma^2)})$, where $g_0=e^2/h$ (a factor of two would be added to account for the spin degree of freedom), V is the voltage drop, and β_d and Σ are the electronic coupling and bulk self energies, respectively, as defined above. These corresponding steady-state currents are confirmed to agree with the long-time limit of the propagation when the applied TD bias is constant for a sufficiently long time. The ac response component is shown to decay due to the bulk dephasing effects. In all cases involving (sufficiently) adiabatic switching, the amplitude of the transient ac response is much smaller than the developed dc. The added bound states are shown to result with persisting oscillations as the bulk is not effective in dissipating their effect on the conductance. We focus, next, on the effect of pulse duration on the conductance.

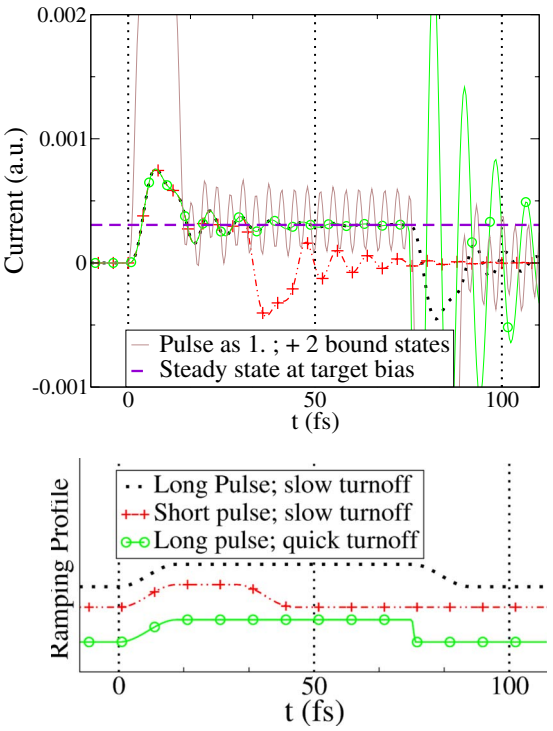

FIG. 3. (Color online) TD conductance $[I(t)]$ due to three different pulses was studied. All pulses correspond to an analytical TD potential bias function, where the same rate is used for the turn on (elapsing 15 fs). They differ in the rate of the turn-off and the length of the pulse at the target bias. An $I(t)$ for a case with bound states is also provided: (i) Black dotted line: slow rate of turn off (15 fs). (ii) Red line with plus symbols: shorter pulse at target. (iii) Green line with circles: fast turn-off pulse (elapsing 1 fs). (iv) Brown fine and solid line: like (i) with two additional bound states. (Bottom) The potential ramping profiles are illustrated.

In Fig. 4 we provide the TD conductance for three pulses that differ only in the length of the pulse. The conductance of the three pulses are shown (right panel) to correspond to the same developing steady state. We are also providing the corresponding $(\bar{t},\bar{\omega})$ Wigner distributions of the current in a form of a projection on a color scheme (left three panels). The current distributions are the integrand in Eq. (44) evaluating the TD expectation value of the current [see Eq. (43)]. In the figure, two rows with varying color-plot scales are provided. In the upper row we use a scale to provide an overall view of the distribution. The switching events' signature is clearly visible. In the lower row we use a smaller scale, highlighting the steady pulse region while including the switching events. The contributions of both the ac and dc components to the steady-state current can now easily be distinguished.

We also note that the Wigner current distributions exhibit quantum broadening (smearing), where, for example, the response to the voltage pulse seems to begin before pulse initiation. This is a direct consequence of time-energy uncertainty principle. A real (quantum) probe cannot provide the behavior of the current energy density at a specific time. This is also evident by observing the current which is obtained by integrating the Wigner current distribution over $\bar{\omega}$ (Fig. 4).

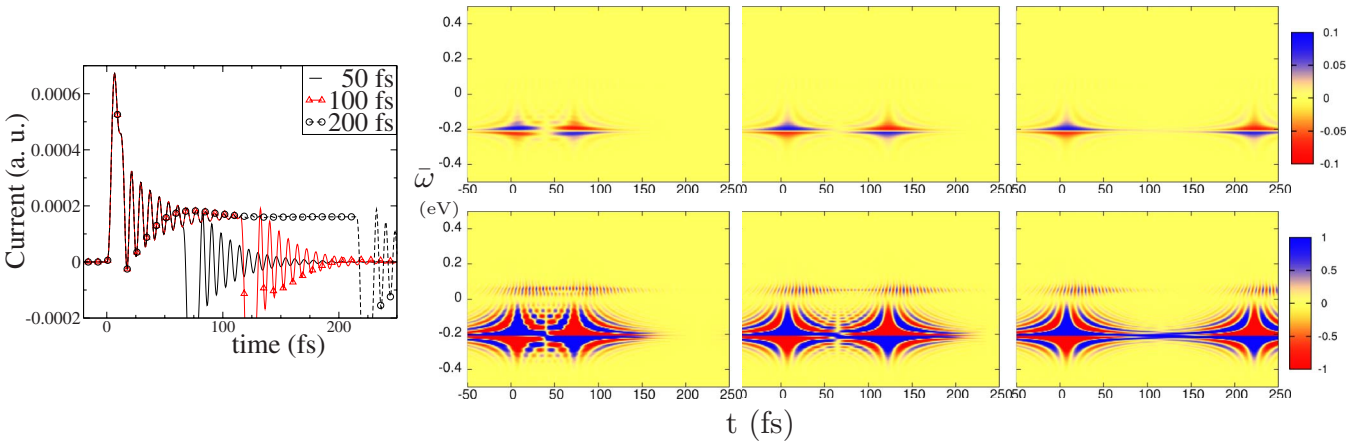

FIG. 4. (Color online) Time span at the target bias study: (i) short (50 fs), (ii) medium (100 fs), and (iii) long (200 fs) pulse. Left panel: $I(t)$ curves. Three right panels: Current distribution with differing color maps between the lower and upper panels.

The current is shown to begin at the correct time as expected for a physical observable. The current distributions provide insight at the quantum-mechanical level on the identified dc and the ringing components of the TD current response.

We focus now on the dc component of the conductance response and analyze it using the current distributions. In Fig. 4 the conductance of the two-site model is shown to be dominated by one open channel. The transient conductance, as observed upon switching on, is shown to emerge from the related band, where the positive sign is associated with the upper portion (in energy) of the band. The lower part of the band is shown to dissipate at long enough time following the switching event leading eventually to the steady state. At the steady state only positive current contributions are noted. The switching off event is essentially characterized by mirroring the band structure of the switch-on event, where the upper part of the band becomes the negative conduction contributions. The ac component as analyzed next emerges due to interferences between the existing channels.

We consider again Fig. 3 focusing on the turn-off event. It is interesting to note that an ac response component may persist over several cycles after the turn-off event depending on the switching rate. For the slower switching rates the number of the ringing oscillations and their amplitudes become smaller. The green curve with circles corresponds to the current under a fast rate for the potential turn off (elapsing 1 fs). This relatively abrupt change leads to a strong ringing mode with amplitudes which exceed the prior dc current by an order of magnitude. This is a very strong oscillating response, and its dissipation may extend over several periods depending on the details of the electronic parameters and the TD details of the perturbation. In addition, the presence of bound states, as shown in the figure, results with the persistence of the ac oscillations. These aspects are further analyzed below.

A strong perturbation applied on a developed steady state leads to a TD current dominated by the ac component. This clearly has an important effect on the functionality of molecular and nanoscale devices. In Fig. 5 we provide several $I(t)$ curves, which demonstrate the dramatic dependence of the decay time on the bias-switching rate. We emphasize that even with the slowest switching case a strong transient negative current upon turn off is observed. The first negative amplitude in absolute value exceeds the prior steady-state current for the relatively slow switching event over 15 fs. The slowest case involving switching over 30 fs reaches about

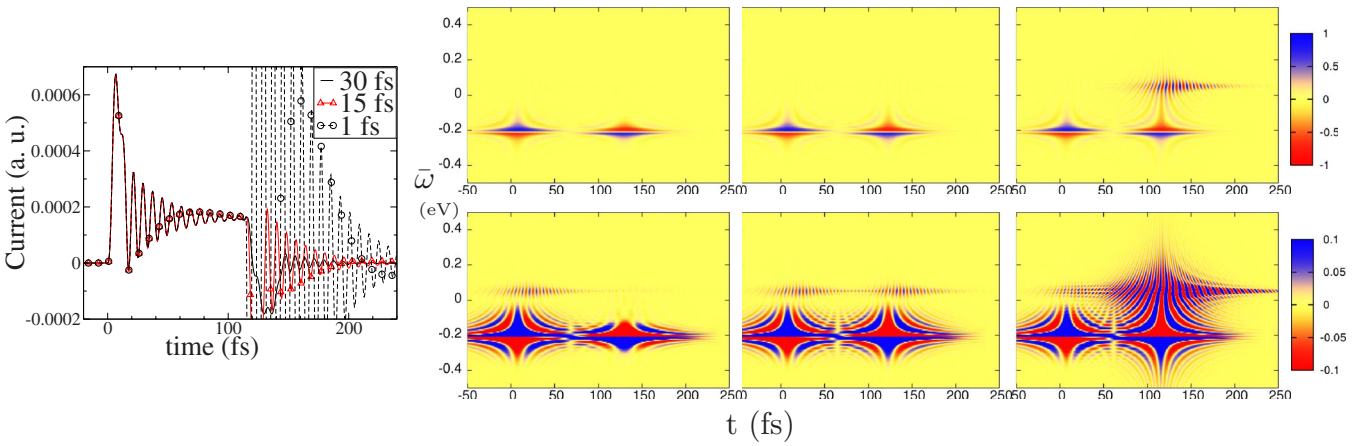

FIG. 5. (Color online) Switch off rate study: (i) slow switching (30 fs), (ii) medium (15 fs), and (iii) quick (1 fs) rates. Left panel: $I(t)$ curves. Three right panels: Current distributions with differing color maps between the lower and upper panels.

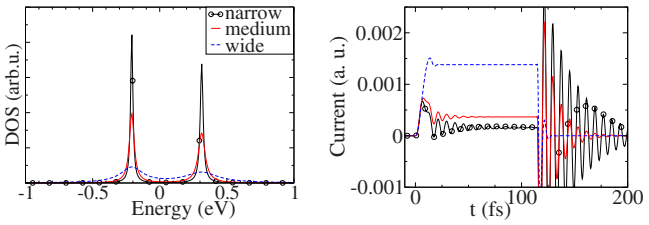

FIG. 6. (Color online) The two-site system with three different broadening (base) factors. (Left) The electronic DOS. (Right) The associated $I(t)$ curves.

the same value as the steady-state current for the same responding amplitude, and shows, as expected, the smallest number of oscillations prior to settling on the zero current. Next, we consider the corresponding Wigner current distributions under differing rates of the turn-off event.

In Fig. 5 we compare the Wigner forms of the current for cases differing significantly in the bias turn-off rate. The Wigner current distribution of the most abrupt case is shown on the rightmost color-map panel. The resulting strong oscillations following the switching event are an order of magnitude larger than the calculated preceding dc values. We, therefore, include (in the lower panel) the current distribution at times where the dc component is still dominant. We use a color-map scale that highlights the ac oscillations in this temporal domain (lower row). The ringing and steady-state ac responses are both concentrated about the same value of $\bar{\omega}$. This value corresponds to an energy shift relative to the electronic level of the propagated state underlying the dc response. An important observation, therefore, is the association of the ac response at steady conditions to the strong ac ringing response due to the relatively abrupt switching event. The shift originates from quantum interference effects as described below. Hence, we focus now on the electronic structure features affecting the dc and ac components.

In order to analyze the origin of this energy shift we consider the electronic structure of conducting channel models involving two sites as used in the TD current calculations. In Fig. 6 (left side) the electronic-energy DOS with three different base values for the broadening (imaginary smear factor parameter) of the bulk GF [see Eq. (36)]. Changing the bulk broadening factor (η_b) allows us to selectively broaden only the open channels. Bound states, which will be explored following the two conducting channels analysis, remain properly unbroaden by this factor. The corresponding TD conductance plots are provided at the right side of the figure. As expected, increasing the broadening results with a larger conductivity at steady state. The $I(t)$ curves also demonstrate the dissipation effects due to the broadening on the conductance oscillatory features. The TD oscillations are shown to dissipate quicker with increasing the broadening. Clearly, upon sufficient broadening of the participating bands in the interference, where, for example, the two channels become one effective band, the oscillatory component of the conduction is almost completely dissipated. We focus next on the energy shift related to the value at which the oscillatory response is observed in the Wigner plots.

The current distributions associate the oscillatory response of the current to interference fringes. The interferences are observed at energy shifts from the open-channel energies determined by the superposition of the two interfering states. This can be understood by simplifying the general propagation expression provided in Eq. (28) assuming that the lesser GF has a peak at bulk affected states ϵ_o [$\mathbf{G}^<(\bar{\omega}) \sim \mathbf{G}^<_{\epsilon_o}\delta(\bar{\omega}-\epsilon_o)$]. We also use Eq. (22) to grossly approximate $G^<(\bar{t},\bar{\omega})$ by

$$ie^{-i(\epsilon_i-\epsilon_j)\bar{t}}\int_{t_0}^{\bar{t}} d\bar{t}'\, e^{i(\epsilon_i-\epsilon_j+2\epsilon_o-2\bar{\omega})\bar{t}'}\tilde{\mathbf{v}}[2(\bar{\omega}-\epsilon_o)]\mathbf{G}^<_{\epsilon_o}. \quad (47)$$

In the last expression, ϵ_i, ϵ_j, and ϵ_o represent bulk affected states (open channels). Interference fringes are, therefore, shifted by $(\epsilon_i-\epsilon_j)/2$ from ϵ_o on the $\bar{\omega}$ axis. Furthermore, they will oscillate in time $\bar{t}$ with frequency $(\epsilon_i-\epsilon_j)$. The interferences that will actually affect the current depend on the unperturbed device's electronic structure and the details of the applied perturbation.

We now turn to focus on systems with bound states added to the open channels. These states do not mix with the bulk electronic structure bands. The bound states *do not* contribute conducting (open) channels coupling the two bulks as they do not mix with the bulk band structure. It is interesting to note recent reports, where bound states are shown to enhance the transient ringing response due to an applied potential pulse.[37,38] We show that bound states can lead to an oscillating response only under certain conditions. These conditions introduce a symmetry-breaking effect where the coherence-driven contribution due to the two interfering bound states involves a relative phase shift between the two states. A simple example for introducing such a shift is provided next.

We consider two systems, where one system includes a symmetric population of the two bound states and the second has only one of the two located below the designated Fermi energy, namely, their population is very different. The bound states are clearly apparent in the electronic DOS, which are plotted in Fig. 7(a). The resulting $I(t)$ plots responding to the (relatively) adiabatic potential pulse are provided in Fig. 7(b). It is shown that persisting oscillations of the current are obtained only for the case with the asymmetry introduced in the population. The current $[I(t)]$ for the other case with both bound states populated is, however, not different from the case which has no bound states added. We next analyze the band structure of the current operator for these systems with the added bound states.

In Figs. 7(c) and 7(d) we provide the Wigner plots of the cases with the symmetric population and the asymmetric population, respectively. For both, the dc band at about −0.25 eV due to the lower-state open channel is observed. The dissipative interference between the two open channels is observed at 0 eV. We then note the contribution due to the populated bound states that is overall vanishing at the switching times. In Fig. 7(c) their interference at −1.0 eV also results in a complete cancellation of the integrated result leading to the current due to the symmetry of the two bound states. Only a symmetry-breaking gating field will lead to a nonvanishing contribution to the current for this interference. This is shown in Fig. 7(d) where the interference of the two

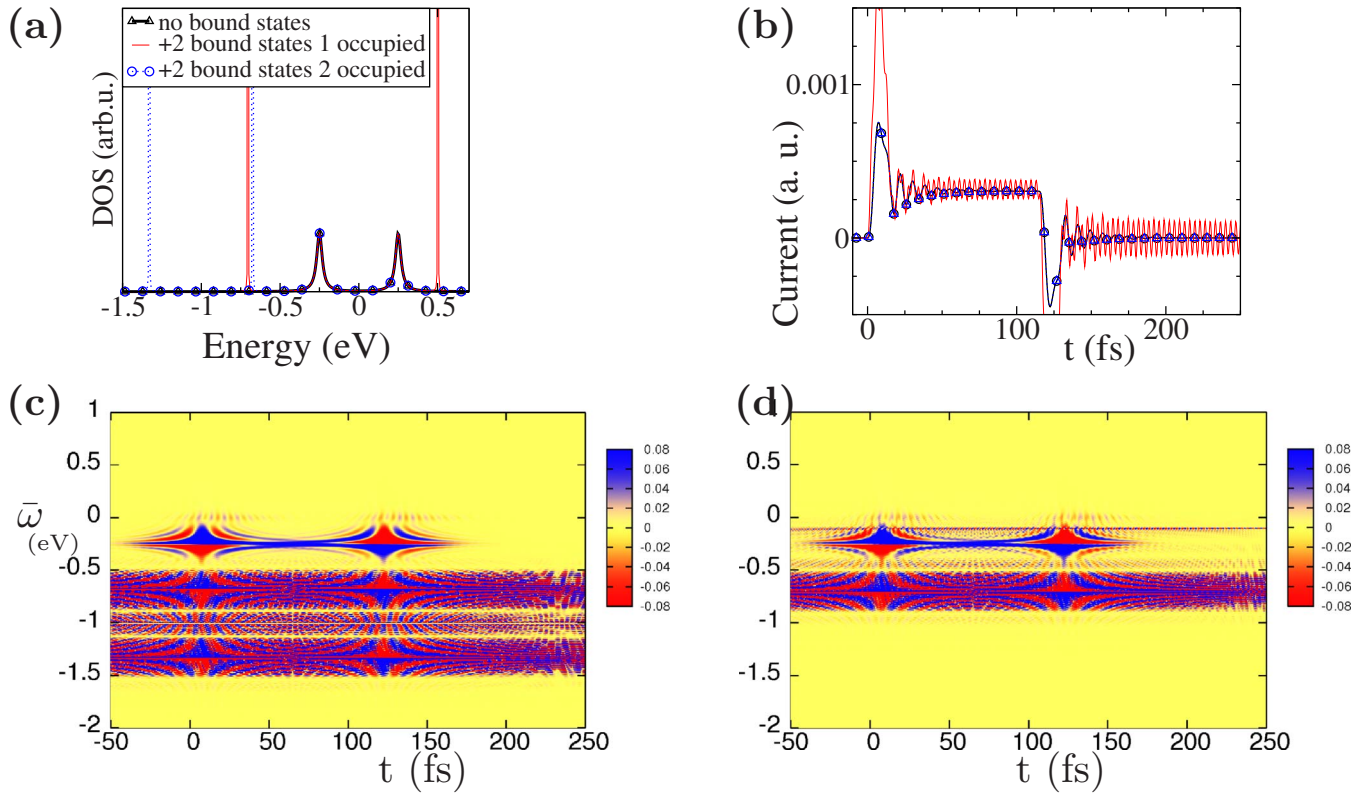

FIG. 7. (Color online) The two-site system including two additional bound states. The interference involving the bound-state results with a persistent current oscillation: (a) the electronic density of states. (b) The $I(t)$ curve. Wigner plot of the current distribution: (c) with two stable bound states, (d) with one stable bound state, and with one unoccupied.

bound states occurs at about −0.1 eV and leads to the persisting oscillation of the current. We describe further in detail the conditions for the bound-state presences leading to oscillation elsewhere.

We now consider the effect of the relative scales of the electronic parameters within the model Hamiltonian on the transient effects of the conductance. The electronic coupling values are related to distances between neighboring sites or relative electronic charge capacities between these sites. All cases considered here involve the relatively adiabatic bias-switching rate (over 15 fs) and a nonadiabatic turn-off event (1 fs). Figure 8 provides the density of states for the different cases of the electronic mixing parameter. We note the bigger splitting around the Fermi energy (FE) and broadening upon the increase of the mixing parameter. Figure 8 also provides TD conductance curves (left) and their corresponding Wigner distributions for the three cases with different electron coupling (β_d) values as specified. The developing dc (steady state) is shown to increase with increasing absolute values of the electronic mixing parameter. This is also associated with a decrease in ac amplitude, where the strongest transient response for the system is observed with the weakest mixing parameter.

We also note that varying the electronic coupling parameters leads to either delocalization or localization of $\bar{t}$ and $\bar{\omega}$ variables in the Wigner current distributions. The Wigner plots show that for the same perturbation the rate of the switch on becomes essentially adiabatic for a large enough electronic coupling value. In addition, a decrease in the electronic coupling parameters leads to localization of the relevant energy range involved in the current-distribution response. Therefore, increasing $|\beta|$ leads to $\bar{t}$ localization and $\bar{\omega}$ delocalization of the current response to the switching. This is the expected dependence on the parameters that control the energy coupling strength between neighboring sites.

As a final aspect of TD conductance, we consider now a two-state system with a driving TD perturbation. The DOS and the related conductance response to a driving ac potential with its frequency tuned exactly to the energy levels difference is illustrated in Fig. 9. We now compare to the current upon applying a symmetry-breaking dc potential bias and treat this as the unperturbed system. The corresponding DOS is shown to result with a slight energy splitting of the two bands. This also leads to reduction of the current, where, however, the broadening ensures that most of the current is not eliminated. More interestingly, a beating frequency is also noted. These two effects are a consequence of the bands being further split which effectively detunes the focused laser field.

The coherence mediated conductance is also analyzed by the current distributions. Two cases are considered. In the upper panel of Fig. 9 the current distributions of the case with only one open channel being occupied are provided. We note that the major contribution to conductance is from the direct interference of the two states as expected. This is what the applied laser is tuned to. An additional current-distribution band is located at the opposite shift from the electronic device state. The shift is defined by the energy

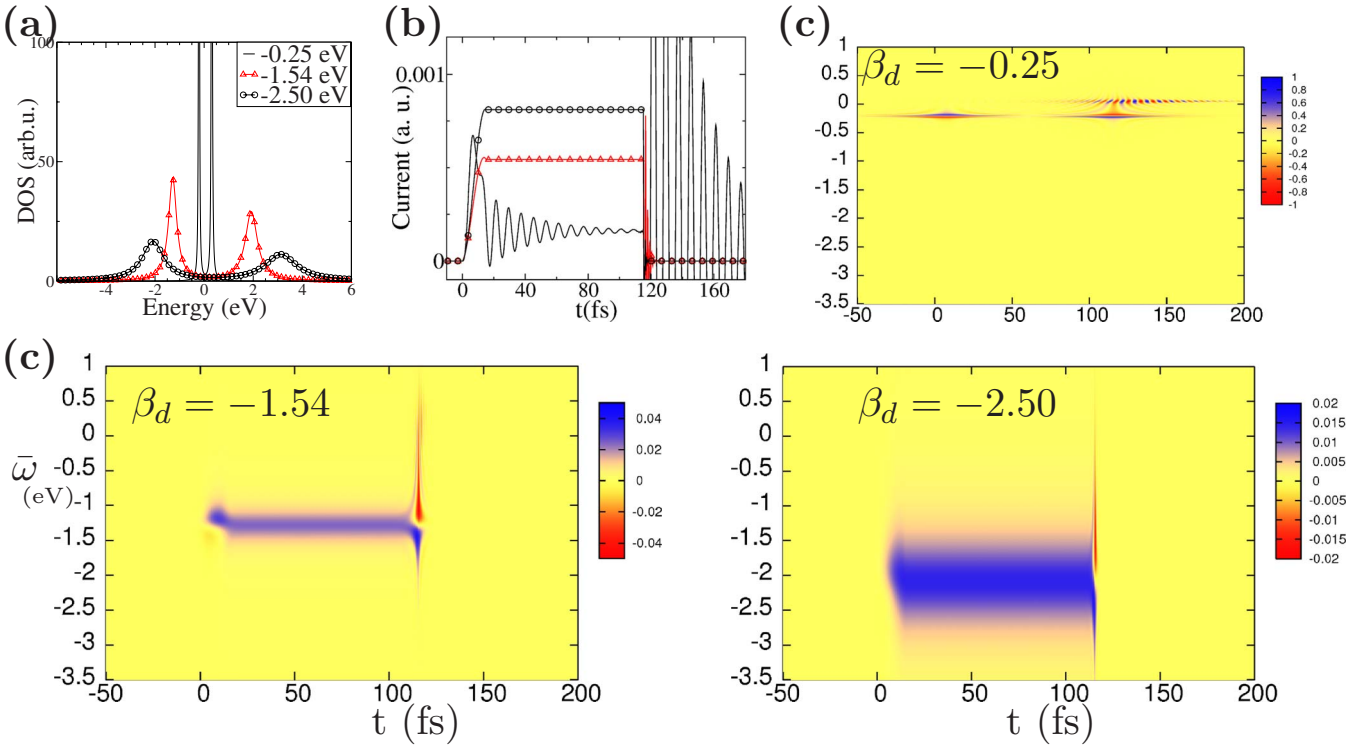

FIG. 8. (Color online) The effect of the strength of electronic coupling (β_d) on TD conductance: (a) the electronic density of states. (b) The $I(t)$ curve. (c) Three Wigner plots of the current distribution for the system including the two additional bound states with the different β_d each with a different color scaling scheme.

average of the two open channels. We note that the opposite shifts (each away from the other state) are shown to contribute substantially to the current. A contribution below the ground state is observed only for the system involving a single-site occupation. In the lower panel, the case with both open channels being populated is considered. For this system an additional band located at the same shift *above* the higher energy open-channel band is introduced. We also note that applying the same ac on the dc-biased system results with a different shift on the two types of the bands. In this case, the

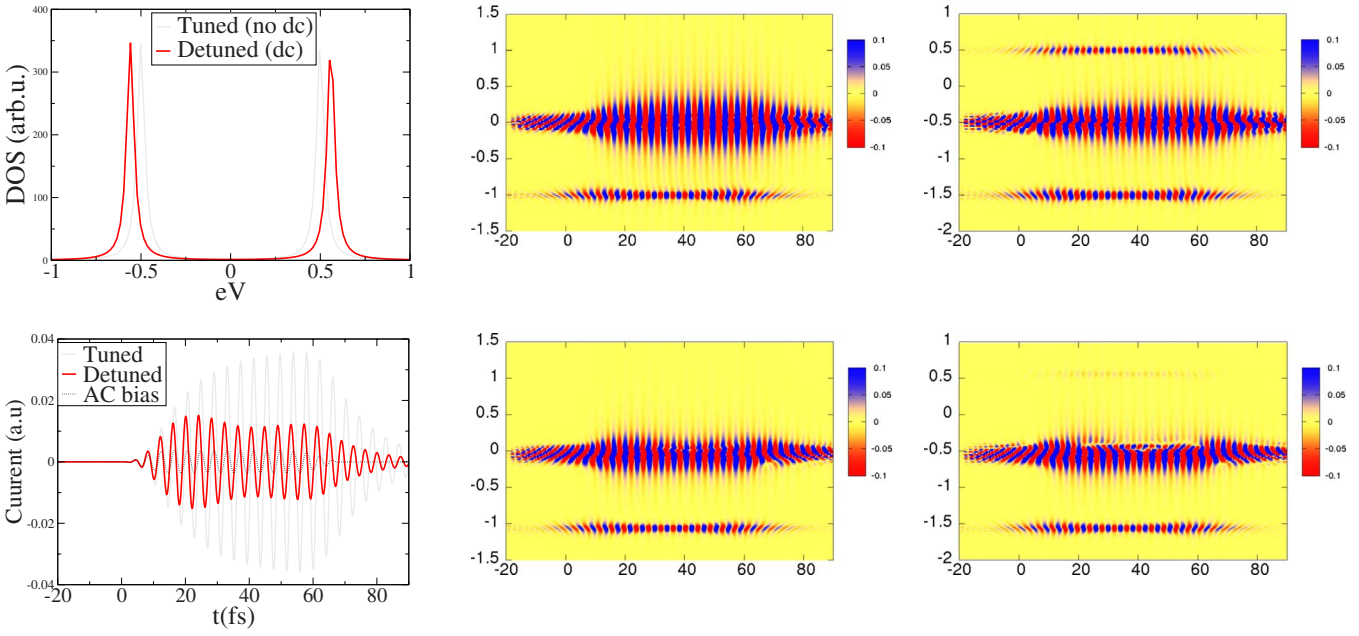

FIG. 9. (Color online) Coherence-driven current of a two-state system with and without a steady dc bias. (Left) The DOS and the *I-t* of the two-state system. Current distribution of: (up) tuned system and (low) dc detuned, and (center) one state occupied and (right) two states occupied

structure of the major shift due to the $\bar{\omega}$ dependence is distorted. This energy dependent shift is responsible to the beating that is observed in the calculated *I-t* curves.

IV. CONCLUSIONS

A formalism based on propagating the K-B electronic e.o.ms is implemented to study transient and TD effects of current through model electronic channels. This is achieved by solving the equations of motion in a mixed time-frequency representation. In this formalism, SE expressions in the energy domain represent the bulk effects on the electronic densities. Namely, bulk-induced broadening effects on the device's electronic structure are directly included in the propagation. We also note that our approach is based on the more physical appropriate nonpartitioned scheme[56] as recently pursued in real-time treatments.[41,45,57]

Our approach by using the SE expressed in the frequency domain avoids the difficulties in propagating open systems in real-time representation. This provides an efficient and reliable framework for including the contact effects on electronic conductance. This provides the opportunity to benefit from highly efficient low-order TD perturbation treatments and to avoid difficulties related to real-time propagations. The effectiveness of the linear response implemented here was confirmed by its ability to reproduce the related steady-state description upon a long enough constant perturbing dc bias. The low-order perturbation treatment is highly useful in addressing weak perturbations where the "bending" of the perturbed electronic states can still be neglected. This approach as implemented, therefore, is useful for studying spectroscopy of open systems and transport under low bias perturbations.

Furthermore, as opposed to approaches based on real-time propagation of density matrices, our approach treats directly the coupling of the device to the bulk system in the propagation. Namely, induced device-based minibands are being propagated. This also allows the resolving of the features within the bulk-induced miniband that determine the transient conductance of the electronic channels. We relate the transient features to quantum interference effects between the device channels or present bound states.

We analyze in detail the interplay between the fundamental electronic parameters and the TD conductance through electronic channels. The parameters include the rate of potential switching event, electronic coupling strength between neighboring sites mediating the electron transfer, and the overall electronic broadening factor representing a host of mechanisms leading to the broadening of the electronic state. Several time-dependent currents and their Wigner current distributions under different applied potential pulses were compared. The system's ability to decay to its equilibrium state after bias turn off, or to achieve a pure dc current at constant bias, was studied. We show that optimization of the dc over ac response (or vice versa) can be attained by controlling the electronic coupling terms and/or shaping the applied TD potential pulse. The tuning of the broadening term was also shown to vary the quantum dephasing effects due to the electrodes and therefore to different decay rates of the ac/ringing response.

The effect of the presence of bound states on the conductance was also studied. The presence of device-bound states may result with long time persisting oscillations, which can dissipate only through other mechanisms. We find that the oscillatory response due to bound state is dependent on a symmetry-breaking scenario between the interfering bound states. Finally we have also studied the coherence-driven ac and the effect of a present dc bias at the unperturbed state. The effect of the dc-induced band shift on the coherence-driven ac response was analyzed using the Wigner form of the current distribution.

ACKNOWLEDGMENTS

B.D.D. acknowledges the Rackham graduate school of the University of Michigan for financial support and for a faculty research award. B.D.D. also acknowledges the Petroleum Research Fund of the ACS (through Grant No. 47118-G6) for financial support. We also acknowledge the National Energy Research Scientific Computing Center (NERSC) of the Department of Energy (DOE) for awarding computing time.

APPENDIX

We begin with the mixed-representation equation of motion of the full system [Eq. (23)]:

$$\frac{\partial}{\partial \bar{t}}\mathbf{G}^{<}(\bar{t},\bar{\omega}) = i[\mathbf{G}^{<}(\bar{t},\bar{\omega}),\mathbf{h}_0] + i\int d\omega'[\mathbf{G}^{<}(\bar{t},\bar{\omega}+\omega')\mathbf{v}(\bar{t},\omega') - \mathbf{v}(\bar{t},\omega')\mathbf{G}^{<}(\bar{t},\bar{\omega}-\omega')]. \tag{A1}$$

where $\mathbf{h}_0=\mathbf{S}^{-1/2}\bar{\mathbf{h}}_0\mathbf{S}^{-1/2}$, $\mathbf{v}(\bar{t},\omega')=\mathbf{S}^{-1/2}\bar{\mathbf{v}}(\bar{t},\omega')\mathbf{S}^{-1/2}$, and $\mathbf{G}^{<}(\bar{t},\bar{\omega})=\mathbf{S}^{1/2}\bar{\mathbf{G}}^{<}(\bar{t},\bar{\omega})\mathbf{S}^{1/2}$. Here $\bar{\mathbf{h}}_0$, $\bar{\mathbf{v}}(\bar{t},\omega')$, and $\bar{\mathbf{G}}^{<}(\bar{t},\bar{\omega})$ are in the AO representation and $\mathbf{S}$ is the AO overlap matrix. We note that Eq. (A1) applies to a system that is infinite in extent. Our goal is to derive an appropriate mixed-representation equation of motion for a finite system under the influence of infinite baths. We will do this by partitioning our system into a device region and two bulk regions:

$$\bar{\mathbf{h}}_0 = \begin{bmatrix} \bar{\mathbf{h}}_{0LL} & \bar{\mathbf{h}}_{0LC} & 0 \\ \bar{\mathbf{h}}_{0CL} & \bar{\mathbf{h}}_{0CC} & \bar{\mathbf{h}}_{0CR} \\ 0 & \bar{\mathbf{h}}_{0RC} & \bar{\mathbf{h}}_{0RR} \end{bmatrix}, \tag{A2}$$

$$\bar{\mathbf{S}} = \begin{bmatrix} \bar{\mathbf{S}}_{LL} & 0 & 0 \\ 0 & \bar{\mathbf{S}}_{CC} & 0 \\ 0 & 0 & \bar{\mathbf{S}}_{RR} \end{bmatrix}, \tag{A3}$$

$$\bar{\mathbf{v}}(t,\omega) = \begin{bmatrix} 0 & 0 & 0 \\ 0 & \bar{\mathbf{v}}_{CC}(t,\omega) & 0 \\ 0 & 0 & 0 \end{bmatrix}, \tag{A4}$$

$$\bar{\mathbf{G}}^{<}(\bar{t},\bar{\omega}) = \begin{bmatrix} \bar{\mathbf{G}}^{<}_{LL}(\bar{t},\bar{\omega}) & \bar{\mathbf{G}}^{<}_{LC}(\bar{t},\bar{\omega}) & 0 \\ \bar{\mathbf{G}}^{<}_{CL}(\bar{t},\bar{\omega}) & \bar{\mathbf{G}}^{<}_{CC}(\bar{t},\bar{\omega}) & \bar{\mathbf{G}}^{<}_{CR}(\bar{t},\bar{\omega}) \\ 0 & \bar{\mathbf{G}}^{<}_{RC}(\bar{t},\bar{\omega}) & \bar{\mathbf{G}}^{<}_{RR}(\bar{t},\bar{\omega}) \end{bmatrix}. \tag{A5}$$

Note that we make the following two important assumptions: first the system-bulk coupling overlap submatrices ($\mathbf{S}_{LC}$, $\mathbf{S}_{RC}$,

etc.) are zero, and second, the TD perturbation is nonzero only in the device (CC) region. This derivation will lead to a generalized quantum master equation (GQME) with memory terms that resemble the weak system bath coupling memory kernel for the density-matrix GQME. Partitioning yields the following equations of motion:

$$i\frac{\partial}{\partial \bar{t}}\mathbf{G}^{<}_{CC}(\bar{t},\bar{\omega}) = [\mathbf{h}_{0CC},\mathbf{G}^{<}_{CC}(\bar{t},\bar{\omega})] + \sum_{I\in L,R}[\mathbf{h}_{CI}\mathbf{G}^{<}_{IC}(\bar{t},\bar{\omega}) - \mathbf{G}^{<}_{CI}(\bar{t},\bar{\omega})\mathbf{h}_{IC}] + \int d\omega'[\mathbf{v}_{CC}(\bar{t},\omega')\mathbf{G}^{<}_{CC}(\bar{t},\bar{\omega}-\omega') - \mathbf{G}^{<}_{CC}(\bar{t},\bar{\omega}+\omega')\mathbf{v}_{CC}(\bar{t},\omega')], \tag{A6}$$

$$i\frac{\partial}{\partial \bar{t}}\mathbf{G}^{<}_{IC}(\bar{t},\bar{\omega}) = \mathbf{h}_{0II}\mathbf{G}^{<}_{IC}(\bar{t},\bar{\omega}) + \mathbf{h}_{0IC}\mathbf{G}^{<}_{CC}(\bar{t},\bar{\omega}) - \mathbf{G}^{<}_{II}(\bar{t},\bar{\omega})\mathbf{h}_{0IC} - \mathbf{G}^{<}_{IC}(\bar{t},\bar{\omega})\mathbf{h}_{0CC} - \int d\omega'[\mathbf{G}^{<}_{IC}(\bar{t},\bar{\omega}+\omega')\mathbf{v}_{CC}(\bar{t},\omega')], \tag{A7}$$

where $I\in L,R$. Furthermore, given the assumptions made on the overlap matrix, we have $\mathbf{v}_{CC}(\bar{t},\omega')=\mathbf{S}^{-1/2}_{CC}\bar{\mathbf{v}}_{CC}(\bar{t},\omega')\mathbf{S}^{-1/2}_{CC}$, $\mathbf{h}_{0IJ}=\mathbf{S}^{-1/2}_{II}\bar{\mathbf{h}}_{0IJ}\mathbf{S}^{-1/2}_{JJ}$, and $\mathbf{G}^{<}_{IJ}(\bar{t},\bar{\omega})=\mathbf{S}^{1/2}_{II}\bar{\mathbf{G}}^{<}_{IJ}(\bar{t},\bar{\omega})\mathbf{S}^{1/2}_{JJ}$ for $I,J\in L,C,R$. In addition, we will assume that the last term in Eq. (A7) is negligible. In studying large chemical systems in the AO representation, this can easily be achieved by extending the dimension of the device beyond the spatial extent of the perturbation (assuming that the perturbation is finite in spatial extent). We now divide the lesser GF into a sum of two parts, as follows,

$$\mathbf{G}^{<}(\bar{t},\bar{\omega}) \equiv \mathbf{G}^{0,<}(\bar{\omega}) + \mathbf{\Delta G}^{<}(\bar{t},\bar{\omega}), \tag{A8}$$

where $\mathbf{G}^{0,<}(\bar{\omega})$ is the lesser GF in the absence of a TD perturbation (i.e., Hamiltonian is constant in time) and $\mathbf{\Delta G}^{<}(\bar{t},\bar{\omega})$ is the remainder (i.e., the part that carries all perturbation effects). The $\mathbf{G}^{0,<}(\bar{\omega})$ is the lesser GF at $\bar{t}=t_0\rightarrow -\infty$. It is merely the contribution to the GF in the absence of a time-dependent perturbation. Note furthermore, that $\mathbf{G}^{0,<}(\bar{\omega})$ does not depend on $\bar{t}$ by definition of the Green's function. This implies that

$$\frac{\partial}{\partial \bar{t}}\mathbf{G}^{0,<}(\bar{\omega}) = 0, \tag{A9}$$

and therefore,

$$\frac{\partial}{\partial \bar{t}}\mathbf{G}^{<}(\bar{t},\bar{\omega}) = \frac{\partial}{\partial \bar{t}}\mathbf{\Delta G}^{<}(\bar{t},\bar{\omega}). \tag{A10}$$

Using these properties and the approximations above, we can rewrite Eqs. (A6) and (A7) in terms of $\mathbf{\Delta G}^{<}(\bar{t},\bar{\omega})$:

$$i\frac{\partial}{\partial \bar{t}}\mathbf{\Delta G}^{<}_{CC}(\bar{t},\bar{\omega}) = [\mathbf{h}_{0CC},\mathbf{\Delta G}^{<}_{CC}(\bar{t},\bar{\omega})] + \sum_{I\in L,R}[\mathbf{h}_{CI}\mathbf{\Delta G}^{<}_{IC}(\bar{t},\bar{\omega}) - \mathbf{\Delta G}^{<}_{CI}(\bar{t},\bar{\omega})\mathbf{h}_{IC}] + \int d\omega'[\mathbf{v}_{CC}(\bar{t},\omega')\mathbf{G}^{0,<}_{CC}(\bar{\omega}-\omega') - \mathbf{G}^{0,<}_{CC}(\bar{\omega}+\omega')\mathbf{v}_{CC}(\bar{t},\omega')] + \int d\omega'[\mathbf{v}_{CC}(\bar{t},\omega')\mathbf{\Delta G}^{<}_{CC}(\bar{t},\bar{\omega}-\omega') - \mathbf{\Delta G}^{<}_{CC}(\bar{t},\bar{\omega}+\omega')\mathbf{v}_{CC}(\bar{t},\omega')], \tag{A11}$$

$$i\frac{\partial}{\partial \bar{t}}\mathbf{\Delta G}^{<}_{IC}(\bar{t},\bar{\omega}) = \mathbf{h}_{0II}\mathbf{\Delta G}^{<}_{IC}(\bar{t},\bar{\omega}) - \mathbf{\Delta G}^{<}_{IC}(\bar{t},\bar{\omega})\mathbf{h}_{0CC} + \mathbf{h}_{0IC}\mathbf{\Delta G}^{<}_{CC}(\bar{t},\bar{\omega}). \tag{A12}$$

We can integrate these equations as suggested in the formalism by redefining $\mathbf{\Delta G}^{<}_{IC}(\bar{t},\bar{\omega})$ as follows:

$$\mathbf{\Delta G}^{<}_{IC}(\bar{t},\bar{\omega}) \equiv e^{-i\mathbf{h}_{0II}(\bar{t}-t_0)}\mathbf{\Delta}\mathcal{G}^{<}_{IC}(\bar{t},\bar{\omega})e^{i\mathbf{h}_{0CC}(\bar{t}-t_0)}. \tag{A13}$$

Upon substitution of definition [Eq. (A13)] into Eq. (A12), we get

$$\mathbf{\Delta G}^{<}_{IC}(\bar{t},\bar{\omega}) = \int_{-\infty}^{\bar{t}} d\bar{t}'\, e^{i\mathbf{h}_{0II}(\bar{t}'-\bar{t})}\mathbf{h}_{0IC}\mathbf{\Delta G}^{<}_{CC}(\bar{t},\bar{\omega})e^{-i\mathbf{h}_{0CC}(\bar{t}'-\bar{t})}. \tag{A14}$$

Note that we begin integrating at $-\infty$ because unlike $\mathbf{v}(t)$, which starts at some finite t_0, $\mathbf{v}(\bar{t},\bar{\omega})$ is potentially infinite in extent. In practice, we would choose a finite lower integration limit with absolute value much larger than $1/\eta$, where η is the smallest broadening in the portion of the density of states that contributes to the relevant dynamics. Equation (A14) together with the property $\mathbf{\Delta G}^{<\dagger}_{IC}(\bar{t},\bar{\omega})=-\mathbf{\Delta G}^{<}_{CI}(\bar{t},\bar{\omega})$ can be substituted into Eq. (A11) to give

$$i\frac{\partial}{\partial \bar{t}}\mathbf{\Delta G}^{<}_{cc}(\bar{t},\bar{\omega}) = [\mathbf{h}_{cc},\mathbf{\Delta G}^{<}_{cc}(\bar{t},\bar{\omega})] + \int d\omega'[\mathbf{v}_{cc}(\bar{t},\omega')\mathbf{G}^{<}_{cc}(\bar{t},\bar{\omega}-\omega') - \mathbf{G}^{<}_{cc}(\bar{t},\bar{\omega}+\omega')\mathbf{v}_{cc}(\bar{t},\omega')] + \int_{-\infty}^{\infty} dt'[\mathbf{\Sigma}^{\mathbf{R}}(\bar{t}-t')\mathbf{\Delta G}^{<}_{\mathbf{cc}}(t',\bar{\omega})e^{-i\mathbf{h}_{cc}(\bar{t}-t')} - e^{i\mathbf{h}_{cc}(\bar{t}-t')}\mathbf{\Delta G}_{\mathbf{cc}}(t',\bar{\omega})\Sigma^{A}(t'-\bar{t})], \tag{A15}$$

where the self energies $\mathbf{\Sigma}^{\mathbf{R}}(t)$ and $\mathbf{\Sigma}^{\mathbf{A}}(t)$ are defined as follows:

$$\mathbf{\Sigma}^{\mathbf{R}}(t) \equiv \sum_{I \in L,R} \mathbf{h}_{0CI}\mathbf{g}^{\mathbf{R}}_{\mathbf{II}}(t)\mathbf{h}_{0IC}, \tag{A16}$$

$$\mathbf{\Sigma}^{\mathbf{A}}(t) \equiv \sum_{I \in L,R} \mathbf{h}_{0CI}\mathbf{g}^{\mathbf{A}}_{\mathbf{II}}(t)\mathbf{h}_{0IC}, \tag{A17}$$

$$\mathbf{g}^{\mathbf{R}}_{\mathbf{II}}(t) \equiv -i\Theta(t)e^{-i\mathbf{h}_{\mathbf{II}}t}, \tag{A18}$$

$$\mathbf{g}^{\mathbf{A}}_{\mathbf{II}}(t) \equiv i\Theta(-t)e^{-i\mathbf{h}_{\mathbf{II}}t}, \tag{A19}$$

where $\Theta(-t)$ is the Heaviside step function. The last two equations are both solutions to

$$\left[i\mathbf{1}\frac{\partial}{\partial t} - \mathbf{h}_{0II}\right]\mathbf{g}_{\mathbf{II}}(t) = \mathbf{1}\delta(t). \tag{A20}$$

One can readily show that the Fourier transforms of the last equation gives the usual equations for the retarded and advanced GFs in the frequency domain.

[1] C. M. Fischer, M. Burghard, and S. Roth, Synth. Met. **71**, 1975 (1995).
[2] M. A. Reed, C. Zhou, C. J. Muller, T. P. Burgin, and J. M. Tour, Science **278**, 252 (1997).
[3] J. Chen, M. A. Reed, A. M. Rawlett, and J. M. Tour, Science **286**, 1550 (1999).
[4] C. P. Collier, E. W. Wong, M. Belohradsky, F. M. Raymo, J. F. Stoddart, P. J. Kuekes, R. S. Williams, and J. R. Heath, Science **285**, 391 (1999).
[5] C. P. Collier, G. Mattersteig, E. W. Wong, Y. Luo, K. Beverly, J. Sampaio, F. M. Raymo, J. F. Stoddart, and J. R. Heath, Science **289**, 1172 (2000).
[6] T. Rueckes, K. Kim, E. Joselevich, G. Y. Tseng, C. L. Cheung, and C. M. Lieber, Science **289**, 94 (2000).
[7] C. Joachim, J. K. Gimzewski, and A. Aviram, Nature (London) **408**, 541 (2000).
[8] A. Nitzan, Annu. Rev. Phys. Chem. **52**, 681 (2001).
[9] J. M. Tour *et al.*, Chem.-Eur. J. **7**, 5118 (2001).
[10] F. R. F. Fan *et al.*, J. Am. Chem. Soc. **124**, 5550 (2002).
[11] J. Park *et al.*, Nature (London) **417**, 722 (2002).
[12] W. J. Liang, M. Shores, M. P. Bockrath, J. R. Long, and H. Park, Nature (London) **417**, 725 (2002).
[13] Y. Luo *et al.*, ChemPhysChem **3**, 519 (2002).
[14] D. M. Adams *et al.*, J. Phys. Chem. B **107**, 6668 (2003).
[15] R. M. Metzger, Chem. Rev. (Washington, D.C.) **103**, 3803 (2003).
[16] A. Nitzan and M. A. Ratner, Science **300**, 1384 (2003).
[17] R. L. McCreery, Chem. Mater. **16**, 4477 (2004).
[18] Y. Xue, S. Datta, and M. A. Ratner, J. Chem. Phys. **115**, 4292 (2001).
[19] P. S. Damle, A. W. Ghosh, and S. Datta, Phys. Rev. B **64**, 201403(R) (2001).
[20] J. Taylor, H. Guo, and J. Wang, Phys. Rev. B **63**, 245407 (2001).
[21] Y. Xue, S. Datta, and M. A. Ratner, Chem. Phys. **281**, 151 (2002).
[22] P. Damle, A. W. Ghosh, F. Zahid, and S. Datta, Chem. Phys. **171**, 225 (2002).
[23] Y. Xue and M. A. Ratner, Phys. Rev. B **68**, 115406 (2003).
[24] M. Brandbyge, J. L. Mozos, P. Ordejon, J. Taylor, and K. Stokbro, Phys. Rev. B **65**, 165401 (2002).
[25] M. Galperin and A. Nitzan, Ann. N.Y. Acad. Sci. **1006**, 48 (2003).
[26] C. Gonzalez, Y. Simon-Manso, J. Batteas, M. Marquez, M. Ratner, and V. Mujica, J. Phys. Chem. B **108**, 18414 (2004).
[27] L. P. Kouwenhoven, S. Jauhar, K. McCormick, D. Dixon, P. L. McEuen, Y. V. Nazarov, N. C. van der Vaart, and C. T. Foxon, Phys. Rev. B **50**, 2019 (1994).
[28] B. J. Keay, S. Zeuner, S. J. Allen, K. D. Maranowski, A. C. Gossard, U. Bhattacharya, and M. J. W. Rodwell, Phys. Rev. Lett. **75**, 4102 (1995).
[29] T. H. Oosterkamp, L. P. Kouwenhoven, A. E. A. Koolen, N. C. van der Vaart, and C. J. P. M. Harmans, Phys. Rev. Lett. **78**, 1536 (1997).
[30] R. López, R. Aguado, G. Platero, and C. Tejedor, Phys. Rev. Lett. **81**, 4688 (1998).
[31] P. Nordlander, M. Pustilnik, Y. Meir, N. S. Wingreen, and D. C. Langreth, Phys. Rev. Lett. **83**, 808 (1999).
[32] G. Platero and R. Aguado, Phys. Rep. **395**, 1 (2004).
[33] B. H. Wu and J. C. Cao, Phys. Rev. B **73**, 205318 (2006).
[34] A.-P. Jauho, N. S. Wingreen, and Y. Meir, Phys. Rev. B **50**, 5528 (1994).
[35] M. P. Anantram and S. Datta, Phys. Rev. B **51**, 7632 (1995).
[36] R. Baer, T. Seidman, S. Ilani, and D. Neuhauser, J. Chem. Phys. **120**, 3387 (2004).
[37] A. Dhar and D. Sen, Phys. Rev. B **73**, 085119 (2006).
[38] G. Stefanucci, Phys. Rev. B **75**, 195115 (2007).
[39] R. Baer and D. Neuhauser, Int. J. Quantum Chem. **91**, 524 (2003).
[40] R. Baer and D. Neuhauser, J. Chem. Phys. **121**, 9803 (2004).
[41] G. Stefanucci and C. O. Almbladh, Phys. Rev. B **69**, 195318 (2004).
[42] D. Neuhauser and R. Baer, J. Chem. Phys. **123**, 204105 (2005).
[43] N. Bushong, N. Sai, and M. Di Ventra, Nano Lett. **5**, 2569 (2005).
[44] K. Burke, R. Car, and R. Gebauer, Phys. Rev. Lett. **94**, 146803 (2005).
[45] S. Kurth, G. Stefanucci, C. O. Almbladh, A. Rubio, and E. K. U. Gross, Phys. Rev. B **72**, 035308 (2005).
[46] N. Sai, M. Zwolak, G. Vignale, and M. Di Ventra, Phys. Rev. Lett. **94**, 186810 (2005).
[47] C. L. Cheng, J. S. Evans, and T. V. Voorhis, Phys. Rev. B **74**, 155112 (2006).
[48] X. Qian, J. Li, X. Lin, and S. Yip, Phys. Rev. B **73**, 035408 (2006).
[49] L. P. Kadanoff and G. Baym, *Quantum Statistical Mechanics* (Benjamin, New York, 1962).
[50] M. Bonitz, *Quantum Kinetic Theory* (Teubner, Stuttgart, 1998).
[51] D. C. Langerth, *Linear and Non-Linear Electron Transport in*

Solids (Plenum, New York, 1976).
[52] G. Baym, Phys. Rev. **124**, 287 (1961).
[53] G. Baym, Phys. Rev. **127**, 1391 (1962).
[54] J. Maciejko, J. Wang, and H. Guo, Phys. Rev. B **74**, 085324 (2006).
[55] G. Stefanucci and C. O. Almbladh, J. Phys.: Conf. Ser. **35**, 17 (2006).
[56] M. Cini, Phys. Rev. B **22**, 5887 (1980).
[57] G. Stefanucci, S. Kurth, A. Rubio, and E. K. U. Gross, Phys. Rev. B **77**, 075339 (2008).
[58] L. Keldysh, Sov. Phys. JETP **20**, 1018 (1965).
[59] N. E. Dahlen, A. Stan, and R. van Leeuwen, J. Phys.: Conf. Ser. **35**, 324 (2006).
[60] A. L. Fetter and J. D. Walecka, *Quantum Statistical Mechanics* (Dover, New York, 2003).
[61] A. Prociuk, B. Van Kuiken, and B. D. Dunietz, J. Chem. Phys. **125**, 204717 (2006).